

# Dimensional crossover in a quantum gas of light

Kirankumar Karkihalli Umesh<sup>a,1</sup>, Julian Schulz<sup>b,2</sup>, Julian Schmitt<sup>c,1</sup>

Martin Weitz<sup>d,1</sup>, Georg von Freymann<sup>e,2,3</sup> and Frank Vewinger<sup>f1</sup>

<sup>1</sup>*Institut für Angewandte Physik, Universität Bonn,*

*Wegelerstrasse 8, 53115 Bonn, Germany*

<sup>2</sup>*Physics Department and Research Center OPTIMAS,*

*RPTU Kaiserslautern Landau, 67663 Kaiserslautern, Germany*

<sup>3</sup>*Fraunhofer Institute for Industrial Mathematics ITWM, 67663 Kaiserslautern, Germany*

(Dated: January 17, 2024)

arXiv:2311.10485v2 [cond-mat.quant-gas] 16 Jan 2024

---

<sup>a</sup> ORCID: 0000-0002-3644-1233

<sup>b</sup> ORCID: 0000-0003-4630-4117

<sup>c</sup> ORCID: 0000-0002-0002-3777

<sup>d</sup> ORCID: 0000-0002-4236-318X

<sup>e</sup> ORCID: 0000-0003-2389-5532

<sup>f</sup> ORCID: 0000-0001-7818-2981

## Abstract

The dimensionality of a system profoundly influences its physical behaviour, leading to the emergence of different states of matter in many-body quantum systems. In lower dimensions, fluctuations increase and lead to the suppression of long-range order. For example, in bosonic gases, Bose-Einstein condensation (BEC) in one dimension requires stronger confinement than in two dimensions. We experimentally study the properties of a harmonically trapped photon gas undergoing Bose-Einstein condensation along the dimensional crossover from one to two dimensions. The photons are trapped in a dye microcavity where polymer nanostructures provide the trapping potential for the photon gas. By varying the aspect ratio of the harmonic trap, we tune from an isotropic two-dimensional confinement to an anisotropic, highly elongated one-dimensional trapping potential. Along this transition we determine the caloric properties of the photon gas and find a softening of the second-order Bose-Einstein condensation phase transition observed in two dimensions to a crossover behaviour in one dimension.

## INTRODUCTION

In the world of manybody physics, it is common knowledge that the number of accessible dimensions profoundly influences the physical behaviour of a system, leading to the emergence of different states of matter at low dimensions (*i.e.*, less than three dimensions). For bosonic gases, as an example, Bose-Einstein condensation (BEC) is possible in lower dimensions only for a sufficiently strong confinement of a power-law trapping potential [1]. While in the two dimensions (2D) a harmonically trapped gas can undergo a phase transition to a Bose-Einstein condensate at finite temperature, this transition in one dimension (1D) is only observed with tighter confining power-law traps. When confining a 1D system within a harmonic trap there is no sharply defined phase transition in the thermodynamic limit to the condensate phase [2], but rather a smooth crossover to a quasi-condensate. In this regime, large thermal and quantum fluctuations in one dimension inhibit the emergence of true long-range order [3, 4]. For finite-size systems, the change from a phase transition in 2D to a crossover in 1D is less pronounced. Moreover, condensation can occur in 1D depending on the strength of interactions and different regimes for quantum-degenerate Bose gases are expected [5]. It is therefore of great interest to study the crossover from three-dimensional (3D) or two-dimensional (2D) systems to the 1D case. For ultracold atomic gases, both

thermodynamic and coherence properties associated with the emergence of quasi-long range order along the *dimensional crossover* from three to one dimension have been studied experimentally [6, 7]. In the case of a strongly interacting Bose gas, where one expects a crossover from Berezinski-Kosterlitz-Thouless type correlations in 2D to Tomonaga-Luttinger liquid correlations [8], the interplay between interactions and dimensionality has been studied [9], and it has been observed that reducing the dimensionality can strongly influence the temperature of the system [10]. For dipolar gases, the transition to the supersolid phase has been studied along the dimensional crossover from one to two dimensions, showing a transition from a continuous to a discontinuous behaviour [11].

Optical quantum gases have in recent years emerged as an alternative platform for quantum gas experiments [12], which are well-suited for the study of the dimensional crossover from 2D to 1D due to the weak or even negligible interaction. In exciton-polariton condensates, correlations in 1D, 2D and 3D have been studied theoretically for an interacting gas [13]. Here, one crosses from long-range order in 3D via a power law in 2D to exponentially decaying first-order phase correlations in the 1D case. Experimentally, e.g. the formation dynamics has been studied for 1D systems [14, 15], and in 1D coupled lattices, a Kardar-Parisi-Zhang (KPZ) scaling for the phase has been observed [16].

In weakly- or non-interacting photon gases, thermalization and condensation in 1D has been observed in doped optical fibers, where the photons thermally populate the longitudinal degree of freedom in a long single mode fibre [17]. To achieve condensation, the initially linear dispersion relation is altered to a sub-linear dispersion using chirped gratings, together with a spectral filter to provide a nontrivial ground state at finite energy. In contrast to this, one can confine photons in a microcavity, effectively freezing out the longitudinal degree of freedom [18]. The transverse degrees of motion can be restricted by in-plane trapping potentials induced by transverse variations in the optical path lengths, either by structuring the cavity mirror surface [19, 20] or the local refractive index [21, 22]. By this, variable potential geometries can be realized, which have, *e.g.*, allowed to study the thermodynamics of 2D Bose gases which contain a few photons or are trapped in box or double well potentials [23–25]. For this system, a continuous change in the thermodynamic properties has been predicted for the harmonically trapped gas when crossing from a 2D to 1D configuration [26, 27], where in contrast to the 2D case no Bose-Einstein condensation is expected [1].

Here, we use a novel technique to confine photons, namely by printing polymer structures on top of one of the cavity mirrors, which allows us to write structures with sizes below the wavelength of the photons. Using this method, we study the transition from two to one dimension for a harmonically trapped gas of photons by varying the aspect ratio of the trapping potential. In our system, thermalization occurs via radiative contact of the photons to a bath of dye molecules, and correspondingly the thermalization mechanism is decoupled from the dimensionality of the trapping potential, in contrast to atomic Bose gases [28, 29]. For all investigated aspect ratios a macroscopic occupation of the ground state is observed as the photon number is increased, which in two dimensions is accompanied by a sharp transition in the chemical potential, while in one dimension we observe a smooth crossover. For the intermediate cases, we observe a gradual softening of the phase transition, which can be associated to an effective (non-integer) dimension of the system.

## REALIZATION

We prepare our photon gas in an optical microcavity consisting of two highly reflective plane mirrors (reflectivity above 99.995% at 580 nm) spaced by approximately 2  $\mu\text{m}$  filled with a dye solution, see Fig. 1a. The confinement in longitudinal direction effectively freezes out this degree of freedom, yielding a minimum energy of  $\hbar\omega_c \approx 2.1$  eV for the photons in the cavity, corresponding to a wavelength of 580 nm. To confine the photons in the transversal direction we printed a polymer microstructure of height  $d(x, y)$  on one of the flat mirrors. The refractive index of the polymer  $n_s$  exceeds the refractive index  $n$  of the dye solution, such that the optical path length locally increases, leading to an attractive potential energy landscape for the photons in the regions where the polymer is deposited with a potential  $V \propto d(x, y)(n - n_s)/n$  [22]. The geometry of the potential is determined by that of the printed structure,  $d(x, y)$ , where the surface curvature of the printed structure translates to the curvature of the trapping potential and the absolute height to its trap depth. For the used dye solvent ethylene glycole ( $n \approx 1.44$ ) and polymer ( $n_s \approx 1.55$ ) [30], we find a trap depth  $V \approx 1.27k_B T$  for the used maximum structure height of approximately 325 nm. The polymer nanostructuring allows us to fabricate parabolic structures with sufficiently strong curvatures in the tightly-confining  $y$ -direction, along which the corresponding harmonic oscillator potential contains only a single bound state, rendering the photon gas system

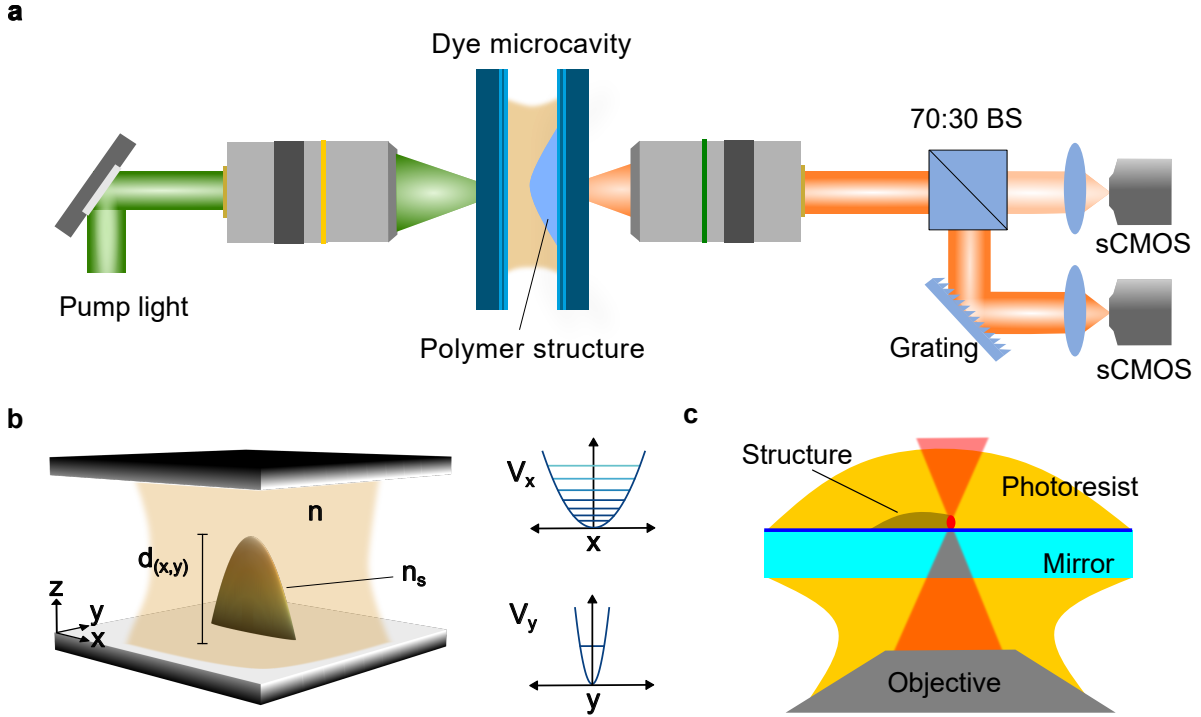


FIG. 1. **a**, Dye-filled microcavity experimental setup. The photon gas is created by pumping the intracavity dye solution using a laser beam spatially shaped using a spatial light modulator (SLM), and focused with a  $10\times$  objective into the microcavity. The cavity consists of two plane mirrors, with a polymer structure printed on one of them to provide a potential for the photons. The cavity emission is sampled using an imaging objective and subsequently analysed either spatially or spectrally. **b**, The polymer structure (refractive index  $n_s$ ) surrounded by dye solution (refractive index  $n$ ) results in a potential for the trapped photon gas. **c**, Direct laser writing scheme, using a focused laser beam to polymerize the photoresist on top of the mirror surface.

effectively one-dimensional (see Fig. 1b).

The polymer structures were fabricated out of the negative-tone photoresist IP-Dip by a direct laser writing (DLW) system (Nanoscribe Photonic Professional GT) [31]. The substrate was prepared in the immersion configuration, which means that during the writing process, the laser was focused by the objective first through an immersion medium (in our case again IP-Dip) and the substrate of the cavity mirror and at last through the thin dielectric Bragg layers into the photoresist (see Fig. 1c). The writing trajectory followed parallel lines along the longer axis of the potentials ( $x$ -direction) with a line distance of

100 nm (along the  $y$ -direction). To manufacture the desired potential  $d(x, y) = h_0 - c_x x^2 - c_y y^2$ , where  $h_0$  denotes the maximum height of the structure and  $c_x$  and  $c_y$  the curvatures along  $x$ - and  $y$ -direction, respectively, at each point the polymer was exposed up to a height given by  $d(x, y)$ . For the different potentials, we keep the geometry approximately fixed along the  $x$ -direction and vary the curvature along the  $y$ -direction. In the following, we label the different potentials by their aspect ratio  $\Lambda = \omega_y/\omega_x = \sqrt{c_y/c_x}$ , with the trap frequencies  $\omega_x$  and  $\omega_y$ . The ratio  $\Lambda$  quantifies the effective dimension of the photon gas [26], where  $\Lambda = 1$  corresponds to an isotropic 2D harmonic oscillator with equal trapping frequency along  $x$  and  $y$  directions, and quasi-1D is reached when the first excited mode of the strongly confined dimension is not trapped in the potential anymore (which in our case also implies  $k_B T < \hbar\omega_y$ ), which in our case is achieved at  $\Lambda \approx 22$ .

To thermalize the photons they are coupled to a thermal bath at ambient temperature  $T = 300$  K, realised by a dye solution filled between the cavity mirrors (see Fig. 1a), similar to previous work [18, 32]. By repeated absorption-emission cycles photons thermalize to the temperature of the dye solution provided thermalization is sufficiently faster than the photon losses, as is the case in our system [32–34]. Correspondingly, the photons populate the energy levels of the transversal degrees of freedom, *i.e.*, the harmonic oscillator levels in  $x$ - and  $y$ -direction, leading to a spectrum with equidistant frequency spacing above the lowest energy mode (called the 'cutoff' energy or frequency) [18]. To prepare the initial photon population and to compensate for losses out of the system we exploit the low reflectivity of our mirrors at 532 nm to inject dye molecular excitation using a laser at 532 nm, which fixes the total photon number  $N$ . The pump light is time modulated with 500 ns pulse width at 50 Hz repetition rate to prevent bleaching of the dye molecules [18]. A spatial light modulator is used to shape the pump laser profile to match the structure size on the mirror, thus reducing unwanted fluorescence from unconfined modes from outside the polymer-based structure.

To analyse the photon gas we collect the light emitted through one of the cavity mirrors, and split the transmitted radiation into two paths after lifting the polarization degeneracy using a polarizer. About 70% of the light is collected by a spectrometer, and 30% are used for spatial imaging of the photon gas. Typical observed density distribution of the photon gas trapped in the 1D to 2D potential are shown in Fig 2, where one can see the density tightly squeezed along the  $y$  direction for 1D ( $\Lambda = 22$ ), elliptic for the 1D-2D ( $\Lambda = 5$ ) potential, and radially symmetric for the isotropic 2D potential ( $\Lambda = 1$ ). The

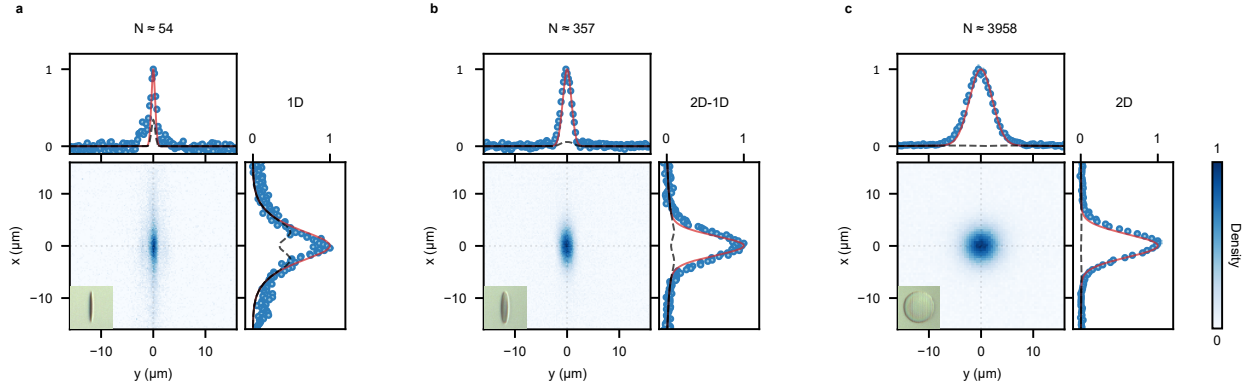


FIG. 2. Density distribution of photons in the quantum degenerate regime in a 1D (**a**,  $\Lambda = 22$ ), 2D-1D (**b**,  $\Lambda = 5$ ) and 2D (**c**,  $\Lambda = 1$ ) harmonic oscillator potentials, respectively. Microscope images of the corresponding polymer structures on the cavity mirror are shown as insets. The dashed lines indicate the position of the cuts through the center of the cloud along the horizontal and vertical axis shown in the side and upper panel. The dashed black line in the cut panels shows the contribution from thermal modes, the solid red line the contribution of the ground mode. For the theoretical expectations we assume a Bose-Einstein distribution of the population within the modes, with the total photon number of  $N = 54$  (1D),  $N = 357$  (2D-1D) and  $N = 3958$  (2D), respectively. The visible deviation in the 1D case is attributed to the emission of free-space modes which are excited at the rim of the potential.

profiles well follow expectations given by a Bose-Einstein distributed population within the bound modes of the harmonic oscillator potential. Especially for the 1D potential, the finite numerical aperture of the objective becomes visible in the diffraction pattern on the sides of the emission, and the visible smearing out along the vertical direction. In the 1D case, one can also observe a broader background below the sharp peak originating from trapped photons, which is attributed to residual fluorescence from free space modes above the harmonic oscillator potential, which lead to an increase in emission at the edge of the potential. As these modes can be separated spectrally, in the following we focus on the spectroscopy of the cavity emission to study the caloric properties of the gas. For this, the emission is dispersed energetically along the  $y$ -direction using an optical grating and imaged onto an sCMOS camera (called *raw spectra* in the following), which allows us to measure both the population in and the spatial profile of individual modes simultaneously, with a spectral resolution of  $\approx 0.08$  THz for the lowest modes. For higher modes with quantum

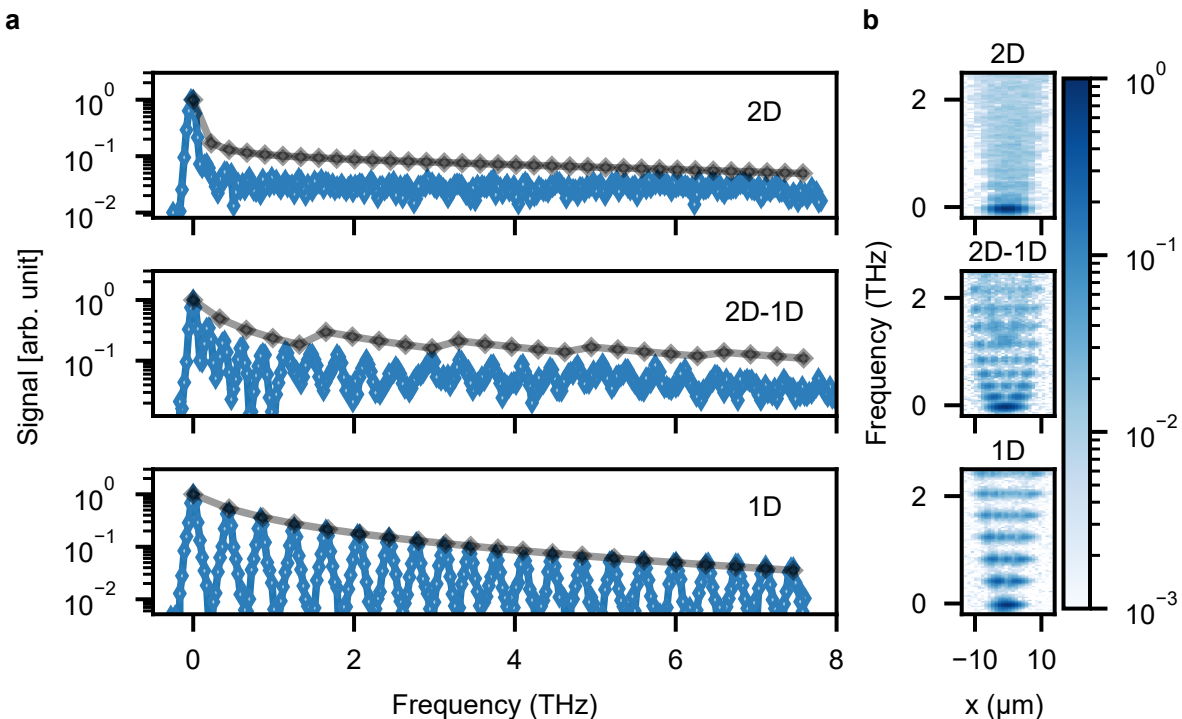


FIG. 3. Photon gas spectroscopy. **a**, The integrated spectrum of the cavity fluorescence for 2D ( $\Lambda = 1$ ), 2D-1D ( $\Lambda = 5$ ) and 1D ( $\Lambda = 22$ ) harmonic oscillator potential and the black curve is the expected Bose-Einstein distribution of photons at  $T = 300$  K, evaluated at the measured position of the harmonic oscillator modes. **b**, Imaging the cavity emission dispersed by a grating onto a camera (raw spectra) allows one to image the shape of the first few modes. For the 2D-1D case the energy states associated with the first excited mode of the tightly confined dimension appear at around the 5th mode. The photon number  $N$  in each case is chosen in the quantum degenerate regime, such that all modes are visible, i.e. the population  $N_0$  in the ground mode does not significantly exceed that of the excited modes, i.e.  $N_0/N \approx 0.3, 0.18$  and  $0.3$  for 2D, 2D-1D and 1D respectively.

numbers  $n_y \gg 1$  the modes start to spatially overlap, correspondingly lowering the resolution for highly excited modes. We extract a spectrum by integrating the obtained raw spectra along the non-dispersed direction, averaging over 20 realizations for a specific total photon number.

Exemplary measured spectra are shown in Fig. 3a for three different aspect ratios, together with the corresponding raw spectra in Fig. 3b obtained by dispersing the cavity



emission using a grating, which retains the mode profile along the x-direction. For the isotropic 2D harmonic oscillator potential with  $\Lambda = 1$  (top panel), one observes equidistantly spaced modes with a frequency spacing of 0.223 THz. In the raw spectra, individual modes  $(n_x, n_y)$  are not resolved, as harmonic oscillator modes with equal  $n_x + n_y$  have the same energy, and correspondingly they overlap spatially. For  $\Lambda = 5$ , corresponding to an anisotropic 2D harmonic oscillator potential with  $\omega_y = 5\omega_x$  (middle panel), one observes equidistantly spaced modes except for the few lowest modes due to slight distortions in the polymer structure. The mode degeneracy increases every 5th mode, as can be seen by the step-like increase in intensity at those modes. In the raw spectrum, this is reflected by the emergence of multiple parabolas corresponding to the different quantum numbers  $n_y$  along the strongly confined  $y$ -direction. One correspondingly finds the emergence of the second dimension ( $n_y = 1$ ) around the 5th mode ( $n_x = 5$ ) along the relaxed  $x$ -direction. The potential with  $\Lambda = 22$  displays 1D harmonic oscillator modes (bottom panel) in the raw spectrum, with an energy spacing of 0.37 THz, and the integrated spectrum correspondingly shows discrete peaks with a degeneracy of one, characteristic for the absence of the second dimension in the recorded energy interval and which is confined by the trap for the strongly asymmetric harmonic oscillator potential, demonstrating that a photon gas trapped in this potential can be considered as being effectively 1D. The photon distribution in all three cases well follows the Bose-Einstein distribution, the black markers in Fig. 3a indicate the expected photon distribution. The theory estimations were calculated using a Bose-Einstein distribution  $g(E) (e^{(E-\mu)/k_B T} - 1)^{-1}$ , with the degeneracy  $g(E)$ . We use the energies of a quantum harmonic oscillator spectrum,  $E = \hbar [\omega_x n_x + \omega_y n_y + \frac{1}{2}(\omega_x + \omega_y)]$ . The trap frequencies  $\omega_x$  and  $\omega_y$  are extracted from the mean mode spacing of the measured spectra, and we truncate the theory spectra by excluding the energy levels which exceed the trap depth inferred from the measured spectrum, and the photon number at each mode is determined by calibrating the signal of the sCMOS camera. The experimental data well follow the theory expectations, apart from a slightly lower mode population for the 2D case, which we attribute to a mismatch in photon number between theory and experiment.

Using the measured spectra, we extract the photon number in the ground mode and the excited modes, respectively, as a function of the total photon number as shown in Fig. 4. Here, one clearly observes a smooth crossover in the ground state population for the 1D case, as expected as in 1D no phase transition to a BEC occurs. The transition becomes sharper

for  $\Lambda = 5$ , and resembles a phase transition for the isotropic 2D potential with  $\Lambda = 1$ . In the latter case, we also observe the saturation of excited modes, as expected for a phase transition from a thermal gas to a Bose-Einstein condensate. For the 1D case, the number of states bound in the potential is smaller than in the 2D case, and correspondingly the softening of the phase transition when crossing from 2D to 1D might also indicate a finite size effect. To investigate this, Fig. 4d shows the theory expectations for a 2D harmonic potential with the same number of energy levels as in the 1D case. While one observes a softening due to finite size effects, the effect is smaller than for the transition to 1D, and correspondingly the experimental data is attributed to give evidence for the dimensional crossover from 1D to 2D. This is also evident in Fig. 3, where no macroscopic population in the ground mode is visible.

The influence of the dimension on the phase transition can be explored by studying the order parameter when tuning the system parameters. As for our case the temperature is fixed at room temperature, the tuning parameter is the total photon number, and we use the absolute value of the chemical potential  $|\mu|$  as an order parameter. To find the chemical potential  $\mu$ , we first extract the internal energy from spectra as in Fig. 3 for different total photon numbers. For each spectrum, we set the ground mode energy to be the zero point energy of the harmonic oscillator,  $E_0 = \hbar(\omega_x + \omega_y)/2$ , count the number of photons in each energy level, multiply by the corresponding mode energy and sum over the whole spectrum, yielding the internal energy as shown in Fig. 5b. For all shown aspect ratios, the internal energy per photon,  $U/N$ , decreases for increasing photon numbers indicating an increasing population in the low-energy states, i.e. the ground mode. As we don't expect a sharp phase transition in 1D (and thus no well-defined critical photon number), for better comparison, each data set is scaled to the photon number  $\tilde{N}$  where the inner energy per particle  $U/N$  changes slope. We extract this number from the theoretical curves based on Bose-Einstein distributed occupations within modes, which yields 611.22, 63.20 and 19.15 photons for the 2D, the 2D-1D and the 1D harmonic oscillator potentials respectively. In the isotropic 2D potential ( $\Lambda = 1$ ), the curve changes slope sharply around  $N/\tilde{N} \approx 1$ , indicating the presence of phase transition, while in the 1D potential ( $\Lambda = 22$ ), the slope changes monotonically, and shows the absence of phase transition features. As for the anisotropic 2D potential ( $\Lambda = 5$ ), the  $U/N$  slope indeed has, although less strong, a sharp change as in 2D isotropic potential Fig. 5.

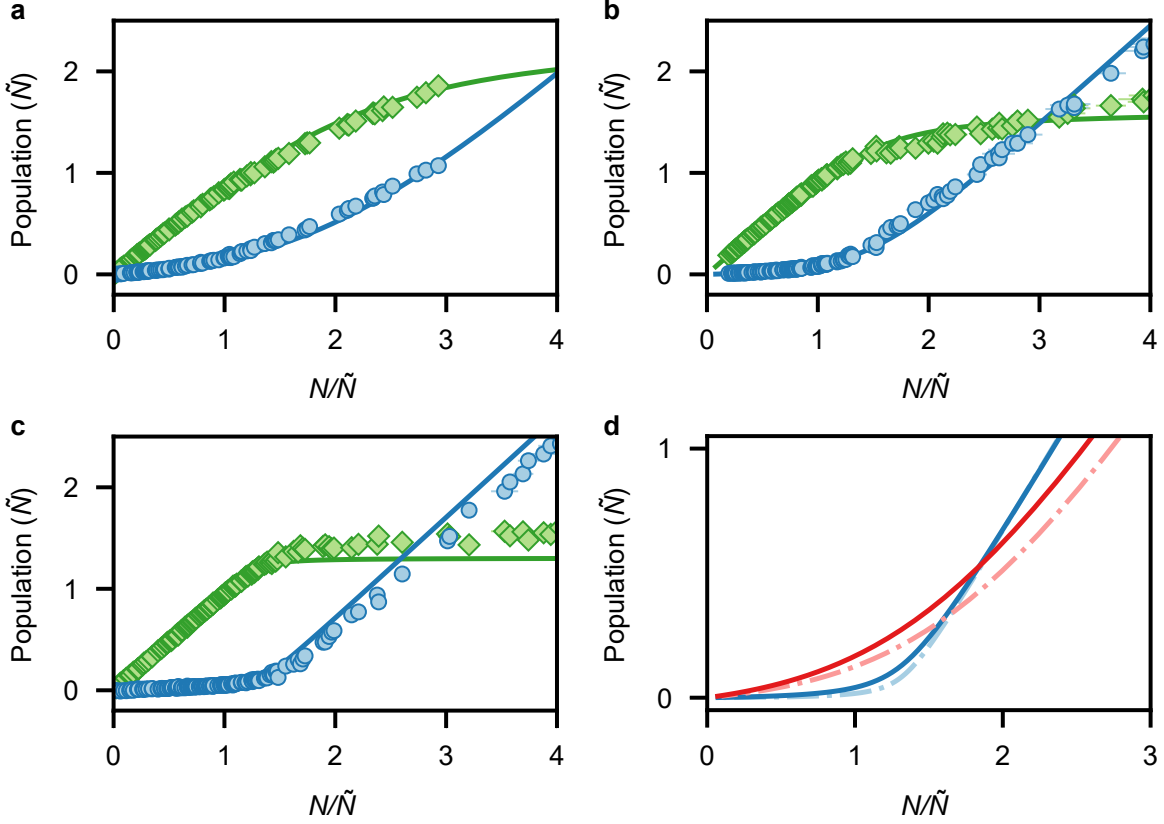


FIG. 4. Softening of the phase transition. **a - c**, show the population in the ground mode (blue dots) and excited modes (green squares), for the 1D case ( $\Lambda = 22$ , **a**, the 1D-2D case ( $\Lambda = 5$ , **b**) and the isotropic 2D potential in **c** for a varying total number of photons. The solid lines give the theory expectations assuming a Bose-Einstein distribution within the modes. Panel **d**, compares the theory expectations for the population in the ground mode for a 1D (red) and a 2D (blue) potential with an equal number of energy levels, with trap depth of  $1.2k_B T$  (solid lines) for finite size system and quasi-infinite system (dash-dot lines) with a depth of  $10k_B T$ . One clearly observes that the effects from the finite size of the system are weaker than the effects of the dimensional crossover. For better comparison, each data set is scaled to the expected photon number  $\tilde{N}$  where the inner energy changes its slope, with  $\tilde{N} = 611.22$ , 63.20 and 19.15 photons for the 2D, the 2D-1D and the 1D harmonic oscillator potentials (see main text). Error bars showing the statistical standard deviations are of the order of the marker size.

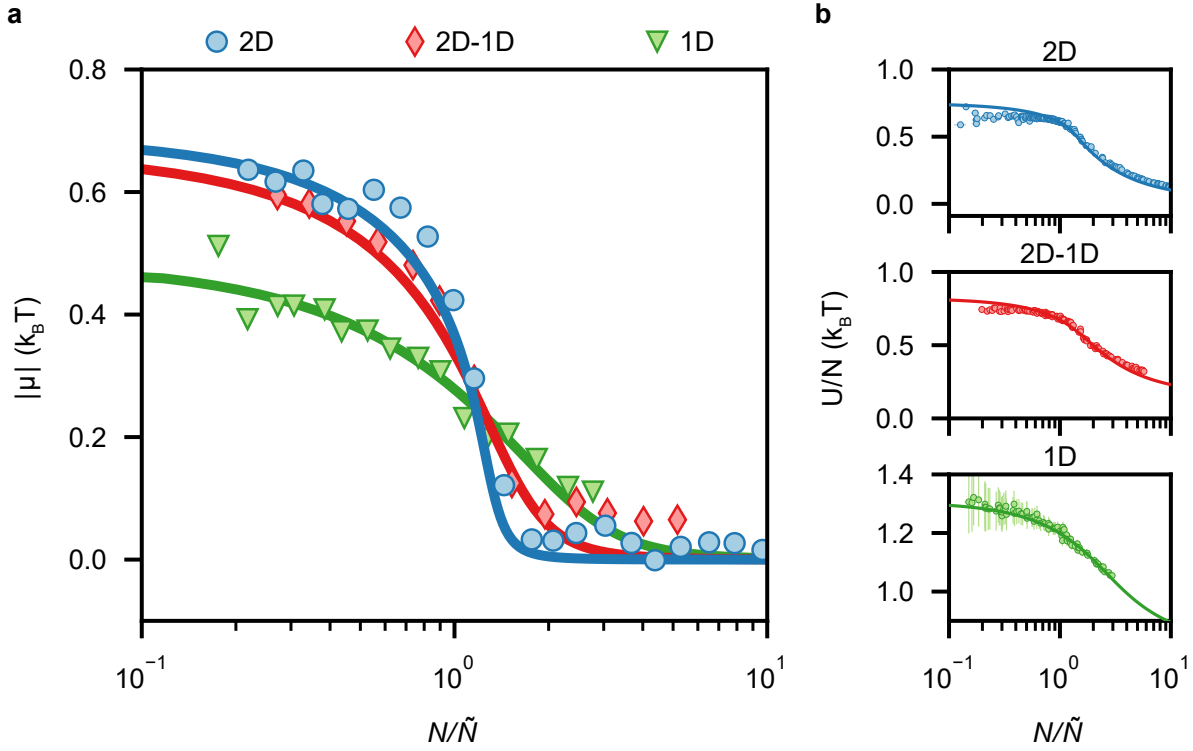


FIG. 5. The change from a phase transition in 2D to a crossover in 1D is visible in the chemical potential. **a**, Symbols represent the measured change in the absolute of chemical potential  $|\mu|$  in the units of thermal energy ( $k_B T$ ), from 1D to 2D (1D, 2D-1D and 2D) harmonic oscillator potentials as function of the normalised photon number  $N/\tilde{N}$ , where the zero-point energy is set to zero. Solid lines are theory expectations for corresponding harmonic oscillator potentials. **b**, The measured internal energy per particle (photon), in units of  $k_B T$ , as a function of the normalised photon number  $N/\tilde{N}$ , from top to bottom, 2D, 2D-1D and 1D harmonic oscillator potential, with their corresponding theory expectations in solid lines. Error bars show statistical standard deviations.

This is visible more strongly in the chemical potential, by numerically taking the partial derivative of the internal energy  $U$  with respect to the photon number  $N$ . The numerical derivative was done by first binning the photon number data for  $U$  (bins of photon number in a geometric series spacing with a common ratio of 1.2, 1.3 and 1.2 for the 2D, the 2D-1D and the 1D harmonic oscillator potentials respectively) to suppress numerical noise. The absolute value of  $\mu$  as expected decreases for all three aspect ratios with increasing photon number. The sharp drop followed by the saturation at the ground state energy for the

isotropic 2D case  $\Lambda = 1$  indicates the expected phase transition in two dimensions, while for increasing  $\Lambda$  we observe a gradual softening of the transition to a continuous crossover for the 1D potential. Thus, the change in the dimension of the potential from 2D to 1D leads to a crossover between the different regimes of the Bose gas instead of a sharp phase transition to a condensate phase.

## CONCLUSIONS

To conclude, we have experimentally studied the dimensional crossover from a 2D isotropic harmonically trapped photon gas to a photon gas confined to 1D around the transition from a thermal to the quantum degenerate case. This crossover is accompanied by a softening of the phase transition, which crosses from a true second-order phase transition to a BEC in 2D to a continuous behaviour in 1D, indicated by the behaviour of the chemical potential and the internal energy of the photon gas for different photon numbers.

For the future, it will be interesting to study different trapping potentials for the photons, and investigate the spatial correlations [35]. While in 1D for the harmonically trapped system no true long-range order is possible, in our finite-size system the correlations can extend over the whole system. In the cavity platform the losses can be tuned from a nearly lossless system to the case of a driven-dissipative condensate by modifying the low-frequency cutoff [36], which is expected to alter the correlations in the system. Also, the structuring method presented here, based on polymer structures within the cavity, allows great flexibility in the design of potentials for photons, ranging from continuous potentials like the ones presented here to tunnel-coupled lattice structures with large tunneling rates. For example, potentials with a logarithmic level spacing have been proposed for factorization of large numbers [37], and in tunnel-coupled potentials, the influence of loss and drive e.g. leads to stable vortices [38, 39], clustering [40] or the emergence of a KPZ-like scaling in the correlations [16], and for 1D chains the emergence of surface states is possible in the presence of a retarded thermo-optic interaction [41].

### Acknowledgements

We acknowledge valuable discussions with E. Stein and A. Pelster. This work has been supported by the Deutsche Forschungsgemeinschaft through CRC/Transregio 185 OSCAR (project No. 277625399). J. Schmitt acknowledges financial support by the EU (ERC, To-

poGrand, 101040409), M. Weitz and J. Schmitt by the Cluster of Excellence ML4Q (EXC 2004/1-390534769).

- 
- [1] V. Bagnato and D. Kleppner, Bose-Einstein condensation in low-dimensional traps, *Phys. Rev. A* **44**, 7439 (1991).
  - [2] W. Ketterle and N. J. van Druten, Bose-Einstein condensation of a finite number of particles trapped in one or three dimensions, *Phys. Rev. A* **54**, 656 (1996).
  - [3] S. Dettmer, D. Hellweg, P. Ryytty, J. J. Arlt, W. Ertmer, K. Sengstock, D. S. Petrov, G. V. Shlyapnikov, H. Kreutzmann, L. Santos, and M. Lewenstein, Observation of phase fluctuations in elongated Bose-Einstein condensates, *Phys. Rev. Lett.* **87**, 160406 (2001).
  - [4] P. Krüger, S. Hofferberth, I. E. Mazets, I. Lesanovsky, and J. Schmiedmayer, Weakly interacting Bose gas in the one-dimensional limit, *Phys. Rev. Lett.* **105**, 265302 (2010).
  - [5] D. S. Petrov, G. V. Shlyapnikov, and J. T. M. Walraven, Regimes of quantum degeneracy in trapped 1d gases, *Phys. Rev. Lett.* **85**, 3745 (2000).
  - [6] A. Vogler, R. Labouvie, G. Barontini, S. Eggert, V. Guarrera, and H. Ott, Dimensional phase transition from an array of 1d luttinger liquids to a 3d Bose-Einstein condensate, *Phys. Rev. Lett.* **113**, 215301 (2014).
  - [7] R. Shah, T. J. Barrett, A. Colcelli, F. Oručević, A. Trombettoni, and P. Krüger, Probing the degree of coherence through the full 1d to 3d crossover, *Phys. Rev. Lett.* **130**, 123401 (2023).
  - [8] H. Yao, L. Pizzino, and T. Giamarchi, Strongly-interacting bosons at 2D-1D dimensional crossover, *SciPost Phys.* **15**, 050 (2023).
  - [9] Y. Guo, H. Yao, S. Ramanjanappa, S. Dhar, M. Horvath, L. Pizzino, T. Giamarchi, M. Landini, and H.-C. Nägerl, Experimental observation of the 2d-1d dimensional crossover in strongly interacting ultracold bosons (2023), arXiv:2308.00411 [cond-mat.quant-gas].
  - [10] Y. Guo, H. Yao, S. Dhar, L. Pizzino, M. Horvath, T. Giamarchi, M. Landini, and H.-C. Nägerl, Cooling bosons by dimensional reduction (2023), arXiv:2308.04144 [cond-mat.quant-gas].
  - [11] G. Biagioni, N. Antolini, A. Alaña, M. Modugno, A. Fioretti, C. Gabbanini, L. Tanzi, and G. Modugno, Dimensional crossover in the superfluid-supersolid quantum phase transition, *Phys. Rev. X* **12**, 021019 (2022).
  - [12] I. Carusotto and C. Ciuti, Quantum fluids of light, *Rev. Mod. Phys.* **85**, 299 (2013).

- [13] A. Chiocchetta and I. Carusotto, Non-equilibrium quasi-condensates in reduced dimensions, *Europhys. Lett.* **102**, 67007 (2013).
- [14] E. Wertz, L. Ferrier, D. D. Solnyshkov, R. Johne, D. Sanvitto, A. Lemaître, I. Sagnes, R. Grousson, A. V. Kavokin, P. Senellart, G. Malpuech, and J. Bloch, Spontaneous formation and optical manipulation of extended polariton condensates, *Nat. Phys.* **6**, 860 (2010).
- [15] M. Wouters, T. C. H. Liew, and V. Savona, Energy relaxation in one-dimensional polariton condensates, *Phys. Rev. B* **82**, 245315 (2010).
- [16] Q. Fontaine, D. Squizzato, F. Baboux, I. Amelio, A. Lemaître, M. Morassi, I. Sagnes, L. Le Gratiet, A. Harouri, M. Wouters, I. Carusotto, A. Amo, M. Richard, A. Minguzzi, L. Canet, S. Ravets, and J. Bloch, Kardar-Parisi-Zhang universality in a one-dimensional polariton condensate, *Nature* **608**, 687 (2022).
- [17] R. Weill, A. Bekker, B. Levit, and B. Fischer, Bose-Einstein condensation of photons in a long fiber cavity, *Opt. Express* **29**, 27807 (2021).
- [18] J. Klaers, J. Schmitt, F. Vewinger, and M. Weitz, Bose-Einstein condensation of photons in an optical microcavity, *Nature* **468**, 545 (2010).
- [19] C. Kurtscheid, D. Dung, A. Redmann, E. Busley, J. Klaers, F. Vewinger, J. Schmitt, and M. Weitz, Realizing arbitrary trapping potentials for light via direct laser writing of mirror surface profiles, *Europhys. Lett.* **130**, 54001 (2020).
- [20] B. T. Walker, B. J. Ash, A. A. P. Trichet, J. M. Smith, and R. A. Nyman, Bespoke mirror fabrication for quantum simulation with light in open-access microcavities, *Opt. Express* **29**, 10800 (2021).
- [21] D. Dung, C. Kurtscheid, T. Damm, J. Schmitt, F. Vewinger, M. Weitz, and J. Klaers, Variable potentials for thermalized light and coupled condensates, *Nature Photonics* **11**, 565 (2017).
- [22] M. Vretnar, B. Kassenberg, S. Bissesar, C. Toebes, and J. Klaers, Controllable Josephson junction for photon Bose-Einstein condensates, *Phys. Rev. Research* **3**, 023167 (2021).
- [23] B. T. Walker, L. C. Flatten, H. J. Hesten, F. Mintert, D. Hunger, A. A. P. Trichet, J. M. Smith, and R. A. Nyman, Driven-dissipative non-equilibrium Bose-Einstein condensation of less than ten photons, *Nat. Phys.* **14**, 1173 (2018).
- [24] E. Busley, L. E. Miranda, A. Redmann, C. Kurtscheid, K. K. Umesh, F. Vewinger, M. Weitz, and J. Schmitt, Compressibility and the equation of state of an optical quantum gas in a box, *Science* **375**, 1403 (2022).

- [25] C. Kurtscheid, D. Dung, E. Busley, F. Vewinger, A. Rosch, and M. Weitz, Thermally condensing photons into a coherently split state of light, *Science* **366**, 894 (2019).
- [26] E. Stein and A. Pelster, Thermodynamics of trapped photon gases at dimensional crossover from 2d to 1d, *New J. Phys.* **24**, 023013 (2022).
- [27] E. Stein and A. Pelster, Photon BEC with thermo-optic interaction at dimensional crossover, *New J. Phys.* **24**, 023032 (2022).
- [28] T. Kinoshita, T. Wenger, and D. S. Weiss, A quantum Newton's cradle, *Nature (London)* **440**, 900 (2006).
- [29] I. E. Mazets, T. Schumm, and J. Schmiedmayer, Breakdown of integrability in a quasi-1d ultracold bosonic gas, *Phys. Rev. Lett.* **100**, 210403 (2008).
- [30] T. Gissibl, S. Wagner, J. Sykora, M. Schmid, and H. Giessen, Refractive index measurements of photo-resists for three-dimensional direct laser writing, *Opt. Mater. Express* **7**, 2293 (2017).
- [31] J. K. Hohmann, M. Renner, E. H. Waller, and G. von Freymann, Three-dimensional  $\mu$ -printing: An enabling technology, *Adv. Opt. Mater.* **3**, 1488 (2015).
- [32] J. Klaers, J. Schmitt, T. Damm, F. Vewinger, and M. Weitz, Bose-Einstein condensation of paraxial light, *Appl. Phys. B: Lasers and Optics* **105**, 17 (2011).
- [33] P. Kirton and J. Keeling, Thermalization and breakdown of thermalization in photon condensates, *Phys. Rev. A* **91**, 033826 (2015).
- [34] J. Schmitt, T. Damm, D. Dung, F. Vewinger, J. Klaers, and M. Weitz, Thermalization kinetics of light: From laser dynamics to equilibrium condensation of photons, *Phys. Rev. A* **92**, 011602 (2015).
- [35] T. Damm, D. Dung, F. Vewinger, M. Weitz, and J. Schmitt, First-order spatial coherence measurements in a thermalized two-dimensional photonic quantum gas, *Nat. Commun.* **8**, 158 (2017).
- [36] F. E. Öztürk, T. Lappe, G. Hellmann, J. Schmitt, J. Klaers, F. Vewinger, J. Kroha, and M. Weitz, Observation of a non-Hermitian phase transition in an optical quantum gas, *Science* **372**, 88 (2021).
- [37] F. Gleisberg, R. Mack, K. Vogel, and W. P. Schleich, Factorization with a logarithmic energy spectrum, *New J. Phys.* **15**, 023037 (2013).
- [38] V. N. Gladilin and M. Wouters, Vortices in nonequilibrium photon condensates, *Phys. Rev. Lett.* **125**, 215301 (2020).



- [39] V. N. Gladilin and M. Wouters, Vortex-pair annihilation in arrays of photon cavities, *Phys. Rev. A* **105**, 013527 (2022).
- [40] R. Panico, P. Comaron, M. Matuszewski, A. S. Lanotte, D. Trypogeorgos, G. Gigli, M. D. Giorgi, V. Ardizzone, D. Sanvitto, and D. Ballarini, Onset of vortex clustering and inverse energy cascade in dissipative quantum fluids, *Nature Photonics* **17**, 451 (2023).
- [41] M. Calvanese Strinati, F. Vewinger, and C. Conti, Nonlocality-induced surface localization in Bose-Einstein condensates of light, *Phys. Rev. A* **105**, 043318 (2022).